

## Lineer Olmayan BEM ve RANS Yöntemleriyle Gemi Pervanelerinin Performans Tahmini

Ahmet Soydan<sup>1</sup>, Şakir Bal<sup>2</sup>

soydan16@itu.edu.tr<sup>1,2</sup>, sbal@itu.edu.tr<sup>2</sup>

<sup>1</sup>Seft Dizayn ve Mühendislik, İstanbul, Türkiye

<sup>2</sup>Gemi İnşaatı ve Gemi Makineleri Mühendisliği Bölümü, İstanbul Teknik Üniversitesi, İstanbul, Türkiye

### ÖZET

Kanat elemanı momentum tekniği, bir pervanenin performans tayininde son derece hızlı, basit ve efektif bir yöntemdir. Geleneksel lineer kanat elemanı momentum yöntemi, direncin indüklenmiş hücum açısı üzerindeki etkisinin küçük olduğunu kabul eder. Dolayısıyla, kanat açıklığı boyunca indüklenmiş hücum açıları küçük kalır. Ancak bu yaklaşımözellikle, yüksek ilerleme sayılarında doğru sonuçlar vermez. Lineer olmayan kanat elemanı momentum teorisi bu problem çözer. Bu çalışmada, DTMB 4381 test pervanesinin açık su performansı kanat elemanı momentum teorisi ve RANS yöntemleriyle incelenmiştir. Elde edilen sonuçlar, lineer kanat elemanları yönteminin sonuçları ve deneysel verilerle karşılaştırılmıştır.

**Anahtar Kelimeler:** Kanat Elemanı Momentum Teorisi, CFD, RANS, Momentum Teorisi, Kanat Elemanı Teorisi, Gemi Pervanesi.

**Makale geçmişi:** Geliş 09/01/2019 – Kabul 30/01/2019

# Performance Prediction of Marine Propellers By Nonlinear Bem and RANS Methods

Ahmet Soydan<sup>1</sup>, Şakir Bal<sup>2</sup>

soydan16@itu.edu.tr<sup>1,2</sup>, sbal@itu.edu.tr<sup>2</sup>

<sup>1</sup>Seft Design and Engineering, Istanbul, Turkey.

<sup>2</sup>Department of Naval Architecture and Marine Engineering, Istanbul Technical University, Istanbul, Turkey

## ABSTRACT

Blade element momentum (BEM) technique is a fast, simple and an efficient method applied to measure the performance of propeller. The traditional linear BEM method is based on the assumption that the drag has a little effect on the induced angle of attack and thus the induced angle of attack is very small at all sections along the blade. However, it is known that this approach creates inaccurate results especially on high advanced ratios. The Nonlinear BEM method avoids this inaccuracy arising from this negligence. In this paper, the open water performance of benchmark propeller DTMB 4381 has been investigated by using the nonlinear BEM and RANS methods. The results have been compared with the linear BEM method and experimental results.

**Keywords:** Blade Element Momentum Theory, CFD, RANS, Momentum Theory, Blade Element Theory, Ship Propeller.

**Article history:** Received 09/01/2019 – Accepted 30/01/2019

## Nomenclature

BEM	: Blade element momentum
c	: Chord length
CFD	: Computational Fluid Dynamics
$C_D$	: Drag coefficient
$C_L$	: Lift coefficient
$C_{L,\alpha}$	: Linear lift curve slope
$C_P$	: Power coefficient
$C_p$	: Pressure coefficient
$C_T$	: Thrust coefficient

DTMB	: David Taylor Model Basin
J	: Advance ratio
$J_i$	: Local induced advance ratio
N	: Number of blades
Q	: Propeller torque
R	: Propeller radius
RANS	: Reynolds Averaged Navier-Stokes
T	: Propeller thrust
$V_\infty$	: Incoming velocity
$\alpha$	: Angle of attack
$\alpha_i$	: Induced angle
$\beta$	: Propeller pitch angle
$\lambda$	: Propeller pitch length
$\Phi$	: Advance angle
$\sigma$	: Solidarity factor
$\omega$	: Angular rotational speed
Re	: Reynolds number

## 1. Introduction

Prediction of hydrodynamic performance of marine propellers has always been a very challenging problem in ship hydrodynamics. CFD (Computational Fluid Dynamics) methods have become very available to solve the problems in the hydrodynamics of marine propellers in recent years. Although the day by day evolution of numerical methods in CFD has been improved significantly, it is still difficult to generate grids to achieve accurate and converged results for rotating propellers and turbine blades. The calculations are very sensitive to grids and boundary conditions. For this reason, when the difficulty of grid generation, long computational times and high costs are taken into consideration, other methods than CFD can be still practical in the preliminary design of marine propellers.

Fast and simple methods can be still applied in the conceptual and preliminary design phases of marine propellers though they have low order accuracy. This usage makes the design process very short. CFD and model testing can be used in the later stages of design process. For instance, lifting surface methods are very simple, fast and efficient approaches to model the cavitating and optimum propellers (Grassi and Brizzolara, 2007, Bal, 2011a and Bal 2011b). Padded propellers were also simulated successfully by a lifting surface technique (Bal and Guner, 2009). Blade element momentum theory is one of these fast and efficient methods. This theory couples the momentum and blade element techniques. In the momentum theory, the actuator disc method is used to represent the propeller. It was originally developed by Rankine. On the other hand, blade element momentum theory has the concept of dividing propeller blade into separate elements (isolated segments) along the radius

(Molland et al, 2011 and Sun et al, 2016). This method was proposed originally by Drzewiecki in 1892. Drzewiecki drew the velocity triangle for each radial section without including velocity induction as reported in (Okulov et al. 2016). The optimum propeller concept was emerged with the development of vortex theory. According to this theory, there is a theoretical maximum value of the energy obtained from the flow. It has an upper limit, which is called the Betz-Joukowsky limit. In 1935, Glauert combined the momentum and blade element theories and developed a conventional blade element momentum theory (Glauert, 1935). More recently, by using Wageningen-B propeller series, a combined blade element momentum theory was implemented for both lightly and moderately loaded marine propellers and the results were with those of three-dimensional RANS solvers (Benini, 2004). All these methods assumed small induced angle of attack at sections along the blade radius. However, it is known that this classical approach gives inaccurate results especially for high advanced ratios. Whitmore and Merrill later developed a correction for nonlinear blade element momentum theory to avoid the inaccuracy arising from linear assumption. This method had better representation for measured propeller performance (Whitmore and Merrill, 2012). Performance of the standard test propeller DTMB4119 was later computed by using blade element momentum theory with Goldstein circulation correction and the results by this approach were compared with those of 3D Navier-Stokes calculations (Ulgen, 2017). In addition, performance factors of the standard test propeller DTMB4119 by using Goldstein circulation correction and Ludweig and Ginzler camber correction were computed by (Karaalioglu and Bal, 2018) and they compared the results with 3D Navier-Stokes calculations (Karaalioglu and Bal, 2018).

In this study, the open water performance of benchmark propeller DTMB 4381 has been investigated by using nonlinear BEM and RANS methods in a way similar to (Soydan, 2018 and Soydan and Bal, 2018). DTMB 4381 propeller has larger number of blades than DTMB 4119. It is known that if the number of blades is increased, BEM methods are not expected to give satisfactory good results due to high interaction between blades. Therefore, the results from nonlinear BEM method are compared with those of experiments and linear BEM method.

## **2. Blade Element Momentum Theory**

Blade element momentum theory couples the momentum approach with blade element method. Momentum theory uses an axisymmetric flow approach to balance the inflow and outflow momentum across the rotor disk. The flow is assumed to be inviscid, irrotational, and incompressible, and the propeller is modeled as an infinitesimally thin disk with a pressure jump across the disk. It also considers an infinite number of propeller blades in the stream tube of propeller. Principles of conservation of energy and axial momentum can be utilized in the momentum theory (Carlton, 2012). The momentum theory, however, does not take the torsional effects into calculations and thus ignores tangential effects. Therefore, energy losses are neglected in this method.

Blade element theory, on the other hand, defines the forces on the blades of a marine propeller as a function of lift and drag coefficients, and the angle of attack of sections. The blade is divided into sufficient number of elements along the radius to obtain a converged solution. Hydrodynamic interaction between elements is neglected and the forces on the blades are assumed to be determined only by the lift and drag characteristics of the sections of the blades. The blade element theory has been developed based on the principle of conservation of angular momentum as well as axial momentum. Blade element momentum theory has been developed by combining the blade element method and momentum theory. In this study, (small angle) analytical solution and nonlinear, large angle solution of blade element momentum theory algorithms given in (Whitmore and Merrill, 2012)

have been applied for simulations of flow around marine propeller. Formulations of both methods are given in the following sections for the completeness of the paper.

## 2.1. Blade Element Theory

Velocity and forces acting on a single blade element are shown in Figure 1. Here  $\beta$  is the local pitch angle. Advance angle is calculated as follows:

$$\Phi = \tan^{-1}\left(\frac{V_\infty}{\omega r}\right) \quad (1)$$

Here  $V_\infty$ ,  $\omega$  and  $r$  are the free stream velocity, rotation rate of propeller and radial position along propeller radius, respectively. Induced angle of attack is defined as:

$$\alpha_i = \beta - \alpha - \Phi \quad (2)$$

where  $\beta$  is the propeller pitch angle and  $\alpha$  is the angle of attack.

The thrust and torque forces of this blade element can then be written as:

$$dT = \frac{1}{2} \rho (V_\infty^2 + (\omega r)^2) (C_L \cos(\alpha_i + \Phi) - C_D \sin(\alpha_i + \Phi)) Nc(r) dr \quad (3)$$

$$dQ = \frac{1}{2} \rho (V_\infty^2 + (\omega r)^2) (C_L \sin(\alpha_i + \Phi) + C_D \cos(\alpha_i + \Phi)) Nc(r) dr \quad (4)$$

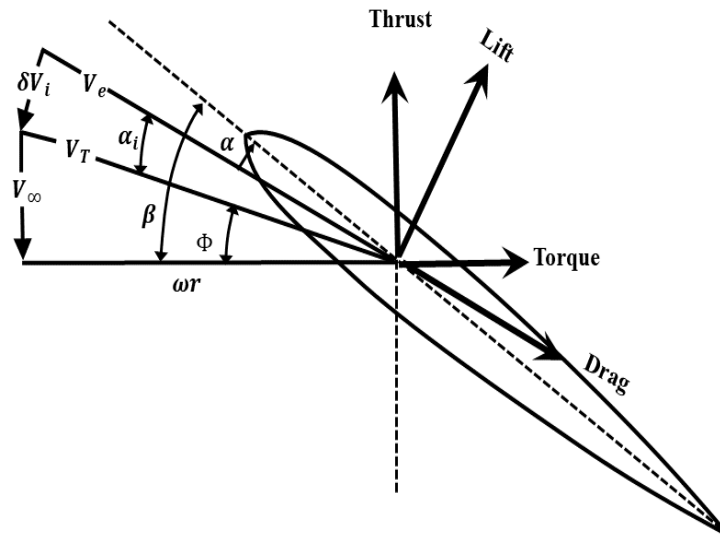


**Figure 1.** Velocity and force diagramme taken from (Whitmore and Merrill, 2012).

Then, these coefficients are integrated to find the total thrust and power coefficient of the propeller as follows (McCormick, 1999):

$$C_T = \int_{x_r}^{x_i} \frac{J^2 + \pi^2 x^2}{8} (C_L \cos(\alpha_i + \Phi) - C_D \sin(\alpha_i + \Phi)) \sigma dx \quad (5)$$

$$C_P = \int_{x_r}^{x_i} \pi \frac{J^2 + \pi^2 x^2}{8} (C_L \sin(\alpha_i + \Phi) + C_D \cos(\alpha_i + \Phi)) \sigma x dx \quad (6)$$

Here,  $\sigma$  is defined as:

$$\sigma = \frac{Nc}{R} \quad (7)$$

The integration limits are taken from propeller root to the propeller tip. For the blade element theory, the propeller diameter, number of blades, pitch and chord distribution must be known. The last factor required to calculate the differential thrust and power coefficient is the induced angle of attack on each radial section. The induced angle of attack is calculated by the momentum theory (Whitmore and Merrill, 2012).

## 2.2. Momentum Theory

The momentum theory is illustrated in Figure 2. Flow is assumed to be incompressible, inviscid and irrotational. First, Bernoulli's equation is applied between the inlet surface and the propeller disk. Later it is applied between the propeller disk and the outlet surface as follows:

$$p_\infty + \frac{1}{2}\rho V_\infty^2 = p + \frac{1}{2}\rho(V_\infty^2 + V_i(r)^2) \quad (8)$$

$$p + \Delta p + \frac{1}{2}\rho(V_\infty^2 + V_i(r)^2) = p_\infty + \frac{1}{2}\rho(V_e^2) \quad (9)$$

Here the differential pressure is defined as,

$$\Delta = \frac{\rho(V_e^2 - V_\infty^2)}{2} \quad (10)$$

Local differential thrust on the propeller disk can be given as,

$$dT = \rho(V_e^2 - V_\infty^2)\pi r dr = \rho(V_e - V_\infty)(V_e + V_\infty)\pi r dr \quad (11)$$

If the momentum balance is applied across the propeller disk,

$$dT + \dot{m}(r)V_\infty = \dot{m}(r)V_e \quad (12)$$

The differential mass flow on the propeller disk is then calculated as follows:

$$\dot{m}(r) = 2\rho(V_e + V_\infty(r))\pi r dr \quad (13)$$

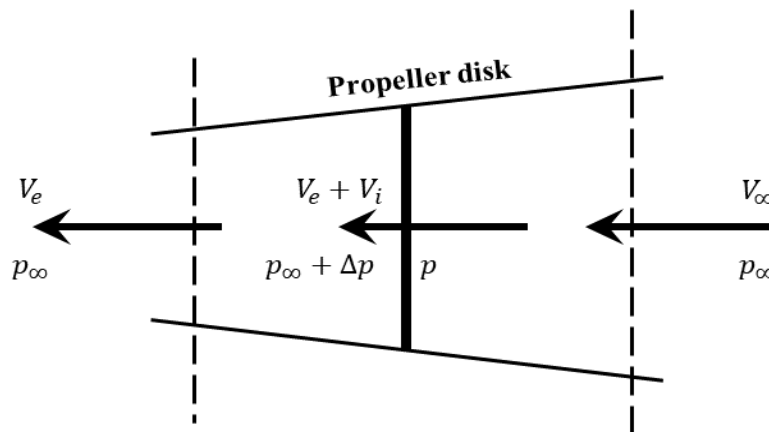


**Figure 2.** Momentum theory taken from (Whitmore and Merrill, 2012).

If equations 12 and 13 are combined, the differential thrust can be written as follows:

$$dT = 2\rho(V_\infty + V_i(r))(V_e - V_\infty)\pi r dr \quad (14)$$

Equations 12 and 14 are combined to obtain the following equation:

$$V_e(r) = V_\infty + 2V_i(r) \quad (15)$$

Equations 14 and 15 can also be combined to get the following equation:

$$dT = 4\rho V_i(r)(V_\infty + V_i(r))\pi r dr \quad (16)$$

Thus the induced velocity in both dimensional and dimensionless forms can be solved as follows, respectively:

$$V_i(r) = \pm \sqrt{\frac{V_\infty^2}{4} + \frac{dT}{4\rho\pi r dr}} - \frac{V_\infty}{2} \quad (17)$$

$$J_i(r) = \sqrt{\frac{J^2}{4} + \frac{1}{\pi x} \frac{dC_T}{dx}} - \frac{J}{2} \quad (18)$$

Equations 16 and 17 can also be combined to get a relationship between thrust and power,

$$C_p = C_T \left( \frac{J}{2} + \sqrt{\frac{J^2}{4} + \frac{2C_T}{\pi}} \right) \quad (19)$$

### 2.3. Analytical (Linear, Small Angle) Solution to Blade Element Momentum Theory

Induced velocity as shown in Figure 1 is given as,

$$\alpha_i = \tan^{-1} \left( \frac{V_i(r)}{\sqrt{V_\infty^2 + (\omega r)^2}} \right) \quad (20)$$

This equation can also be written as follows.

$$\alpha_i = \tan^{-1} \left( \frac{J_i(r)}{\sqrt{J^2 + \pi^2 x^2}} \right) \quad (21)$$

If it is assumed that the drag has little effect on the induced angles, the induced angle is therefore small at all sections along the blade (McCormick, 1999):

$$\alpha_i \ll \Phi \quad (22)$$

The differential thrust on the blade element could be expressed as,

$$dT = \frac{1}{2} \rho (V_\infty^2 + (\omega r)^2) C_L N c(r) dr \quad (23)$$

Equations 16 and 23 can be combined to get the following equation,

$$\alpha_i^2 + \alpha_i \left( \frac{V_\infty}{\omega r} + \frac{C_{L,\alpha} Nc}{8\pi r} \sqrt{1 + \left( \frac{V_\infty}{\omega r} \right)^2} \right) - \frac{C_{L,\alpha} Nc}{8\pi r} \sqrt{1 + \left( \frac{V_\infty}{\omega r} \right)^2} (\beta - \phi) = 0 \quad (24)$$

The closed form solution is as follows,

$$\alpha_i^2 = -\frac{1}{2} \left( \frac{V_\infty}{\omega r} + \frac{C_{L,\alpha} Nc}{8\pi r} \sqrt{1 + \left( \frac{V_\infty}{\omega r} \right)^2} \right) + \frac{1}{2} \sqrt{\left( \frac{V_\infty}{\omega r} + \frac{C_{L,\alpha} Nc}{8\pi r} \sqrt{1 + \left( \frac{V_\infty}{\omega r} \right)^2} \right)^2 + \frac{C_{L,\alpha} Nc}{8\pi r} \sqrt{1 + \left( \frac{V_\infty}{\omega r} \right)^2} (\beta - \phi)} \quad (25)$$

The induced angle is solved for each section and Equations 5 and 6 are then used to calculate the propeller thrust and power coefficients.

#### 2.4. Nonlinear (Large Angle) Solution to Blade Element Momentum Theory

Analytical BEM method assumes that the induced angle of attack is small at all sections along the blade radius and has little effect on drag. However, this approach gives inaccurate results especially for high advanced ratios. Nonlinear BEM method avoids this inaccuracy. In this method there is no assumption on induced angles of attack. In the nonlinear BEM method, a series of equations is iteratively solved until the exact induced angle of attack converges for each blade element. The initial induced angle of attack is calculated by analytical method (linear solution). Then, the derivative of thrust coefficient with respect to  $x$  is solved. This derivative is used to find the induced velocity. Later, the induced velocity is used to calculate the new induced angle of attack. The iterative process is defined in the following equations:

$$\frac{dC_T}{dx} = \frac{J^2 + \pi^2 x^2}{8} (C_L \cos(\alpha_i + \Phi) - C_D \sin(\alpha_i + \Phi)) \sigma \quad (26)$$

$$J_i(r) = \sqrt{\frac{J^2}{4} + \frac{1}{\pi x} \frac{dC_T}{dx} - \frac{J}{2}} \quad (27)$$

$$\alpha_i = \tan^{-1} \left( \frac{J_i(r)}{\sqrt{J^2 + \pi^2 x^2}} \right) \quad (28)$$

In blade element momentum theory, the lift ( $C_L$ ) and drag ( $C_D$ ) coefficients of the blade sections must be determined to calculate the performance factors of the propeller. For this purpose, a program of Nonlinear BEM developed in Python 3.6 programming language. It takes these values (lift and drag coefficients) from XFOIL program for the Reynolds number of each section. XFOIL is an open source FORTRAN code, developed by MIT. It can be used to design and analyze the incompressible/compressible viscous flow over an arbitrary airfoil sections particularly in low Reynolds numbers. More detailed information can be found in (Url-1, 2018). The flow diagram of nonlinear BEM method is also shown in Figure 3.

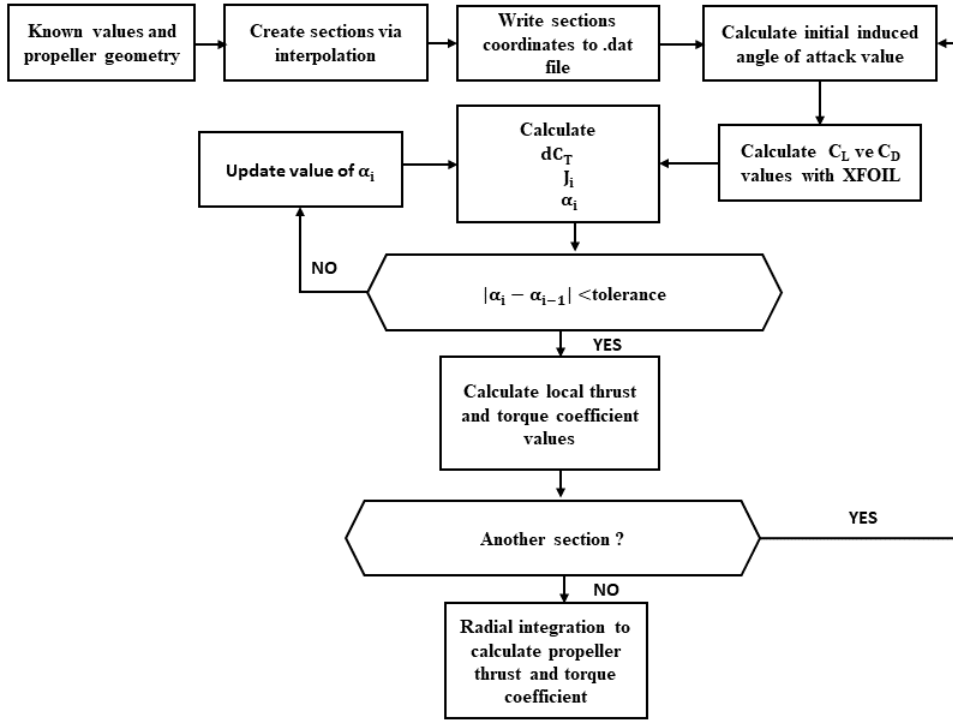


**Figure 3.** Large angle solution algorithm of nonlinear BEM method.

### 3. RANS Calculations

The governing equations for RANS (Reynolds Averaged Navier-Stokes) solver are based on the conservation of mass (continuity) and the momentum values. The flow is assumed to be time independent, three-dimensional, viscous and incompressible (Versteeg and Malalasekera, 2007). The continuity equation is given as:

$$\frac{\partial U_i}{\partial x_i} = 0 \quad (29)$$

and the momentum equation is as follows:

$$\frac{\partial(U_i U_j)}{\partial x_j} = -\frac{1}{\rho} \frac{\partial P}{\partial x_i} + \frac{\partial}{\partial x_j} \left[ \nu \left( \frac{\partial U_i}{\partial x_j} + \frac{\partial U_j}{\partial x_i} \right) \right] - \frac{\partial \overline{u_i' u_j'}}{\partial x_j} \quad (30)$$

Here  $U_i$  and  $u_i'$  are the mean velocity and the fluctuation velocity components in the directions of the Cartesian coordinates  $x_i$ , respectively.  $P$  is the mean pressure,  $\rho$  the density and  $\nu$  the kinematic viscosity of the fluid. The well-known  $k-\varepsilon$  turbulence model is used to model the turbulent flow. The Reynolds stress tensor can then be calculated as follows;

$$u_i' u_j' = -\nu_t \left( \frac{\partial U_i}{\partial x_j} + \frac{\partial U_j}{\partial x_i} \right) + \frac{2}{3} \delta_{ij} k \quad (31)$$

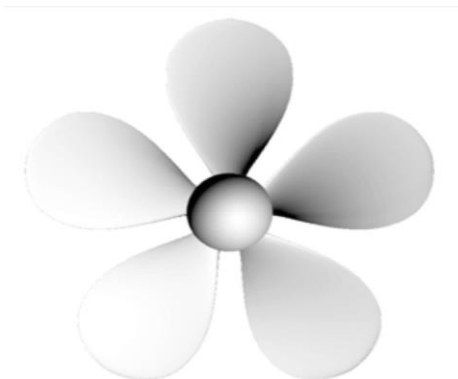
where,  $\nu_t$  is the eddy viscosity,  $\nu_t = C_\mu k^2 / \varepsilon$ .  $C_\mu$  is an empirical constant.  $k$  is the turbulent kinetic energy and  $\varepsilon$  is the turbulent dissipation rate. Details for the  $k-\varepsilon$  turbulence model can be found in (Wilcox, 1993).

### 3.1. Geometry and Boundary Conditions

DTMB 4381 is selected as the test propeller since it has 5 blades. It is expected to show that nonlinear BEM method gives accurate results for even higher number of blades. If the number of blades is increased, the interaction between blades will also increase and the BEM method is not expected to provide satisfactorily good results. So this hypothesis is checked out here. The propeller has no skew and no rake. Its diameter is 0.3048 meters. DTMB4381 propeller, as given below in Table 1, are designed with NACA 66 modified profile and  $a=0.8$  camber line. 3-D model of the propeller is shown in Figure 4.

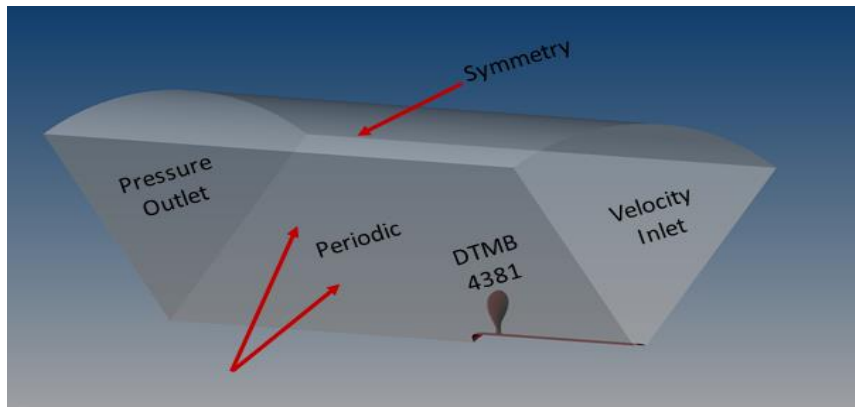
**Table 1.** DTMB4381 Propeller Geometry (Brizzolara et al., 2008).

$r/R$	$c/D$	$P/D$	$t_{max}/c$	$f_{max}/c$
0.20	0.1740	1.3320	0.0351	0.2494
0.25	0.2020	1.3380	0.0369	0.1960
0.30	0.2290	1.3450	0.0368	0.1563
0.40	0.2750	1.3580	0.0348	0.1069
0.50	0.3120	1.3360	0.0307	0.0769
0.60	0.3370	1.2800	0.0245	0.0567
0.70	0.3470	1.2100	0.0191	0.0421
0.80	0.3340	1.1370	0.0148	0.0314
0.90	0.2800	1.0660	0.0123	0.0239
0.95	0.2100	1.0310	0.0128	0.0229
1.00	0.0010	0.9950	0.0123	0.0160



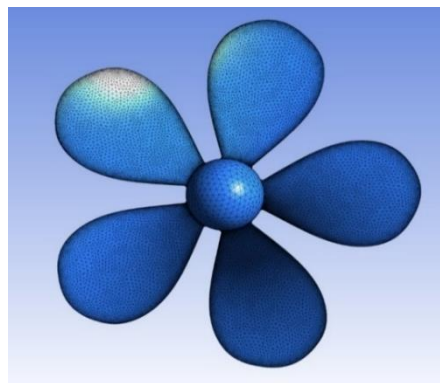
**Figure 4.** DTMB 4381 propeller geometry.

Figure 5 shows the computational domains and boundary conditions. To reduce the computational time, only one blade is modelled to take the advantage of axial symmetry of the flow and periodic boundary condition is used. The right and left sides of the computational domain have been defined as the velocity inlet and pressure outlet, respectively. The propeller and shaft surfaces have been defined as no slip wall to impose the kinematic boundary condition. The upper surface has been defined as symmetry plane.



**Figure 5.** Geometry and boundary conditions.

The computational domain consists of unstructured tetrahedral elements. Figure 6 shows the unstructured tetrahedral mesh generated on the propeller in open water.



**Figure 6.** Unstructured mesh around propeller.

### 3.2. Grid Convergence and Solution Strategy

Three different mesh have been generated for verification and validation study. Uncertainty analysis has been applied with Grid Convergence Index (GCI) as recommended by ITTC for CFD verification (ITTC, 2011). Grid length refinement has been selected greater than 1.3 as recommended in (Celik et al., 2008) and (Roache, 1998). The number of elements are given below in Table 2.

**Table 2.** Number of grids.

Grid Type	Number of Elements
Course	650,981
Medium	946,006
Fine	1,564,694

Advanced coefficient ( $J$ ) is taken as 0.889 (design point) for Uncertainty analysis and Convergence condition ( $R$ ) has been calculated as 0.571. This means that the solution is converging monotonically. The uncertainty value has been calculated as 0.71% and is given in Table 3. Medium grid has been selected to consider the computational time and all analysis have been carried out with medium grid.

**Table 3.** Uncertainty value for open water analysis.

Analysis Set	%GCI <sub>FINE</sub>
1 2 3	0.71

After verification study, the Thrust Coefficient ( $K_T$ ) of the propeller has been validated with the experimental data for  $J=0.889$ . The comparison of the CFD results with experimental data is given in Table 4. Relative difference between numerical and experimental results have been found as -3.846%.

**Table 4.** Comparison of the numerical and experimental results

	CFD	Experiment	Relative Difference (%)
$K_T$	0.200	0.208	-3.846

The ANSYS Fluent 17.2 program has been used for the RANS solution. As the turbulence model,  $k - \epsilon$  turbulence model has been used.  $y +$  value has been kept between 30-300 (Fluent 17.2 User's Manual, 2016).

The second order upwind scheme has been used for the momentum and turbulence terms, and the simple algorithm for velocity pressure interaction has been selected.

#### 4. Results and Discussion

Linear and nonlinear BEM methods and experimental tests of DTMB4381 propeller are shown in Figure 7. Experimental data have been taken from (Brizzolara et al., 2008). As shown in Figure 7, the results of nonlinear method agree well with those of experiments, except at low advance coefficients. On the other hand, linear method over predicts the thrust and torque coefficients especially at high advanced ratios, as expected. For the definitions of  $K_T$  and  $K_Q$ , refer to (Carlton, 2012).

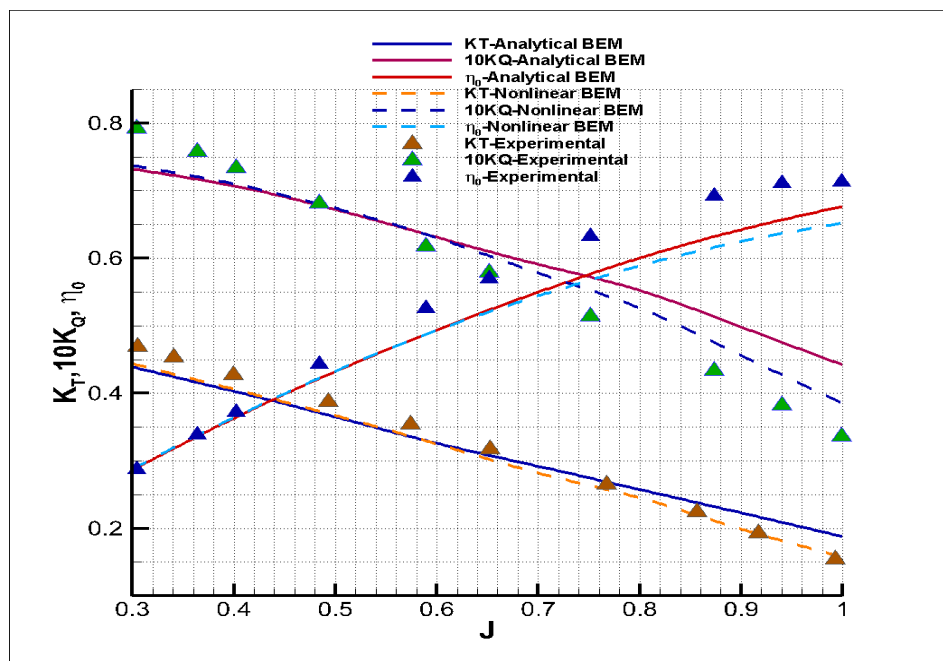


**Figure 7.** Comparison of  $K_T$ ,  $10K_Q$  and  $\eta_0$  values using analytical and nonlinear BEM solutions with experimental data of DTMB 4381.

RANS solution of DTMB4381 propeller is also shown in Figure 8. Computational results agree very well with those of experiments. Figure 9 shows also  $y^+$  distribution around DTMB 4381 for  $J= 1.0$ . Averaged  $y^+$  value is around 90. Figure 10 shows on the other hand the pressure distribution around DTMB 4381 for  $J=0.889$ .

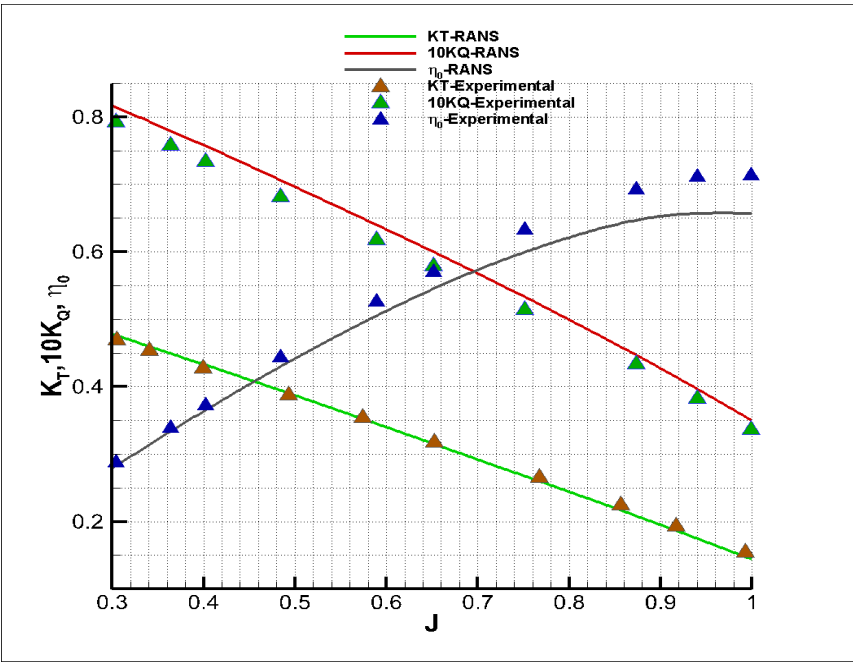


Figure 8.  $K_T$ ,  $10K_Q$  and  $\eta_0$  values by both RANS solution and experiments of DTMB 4381.

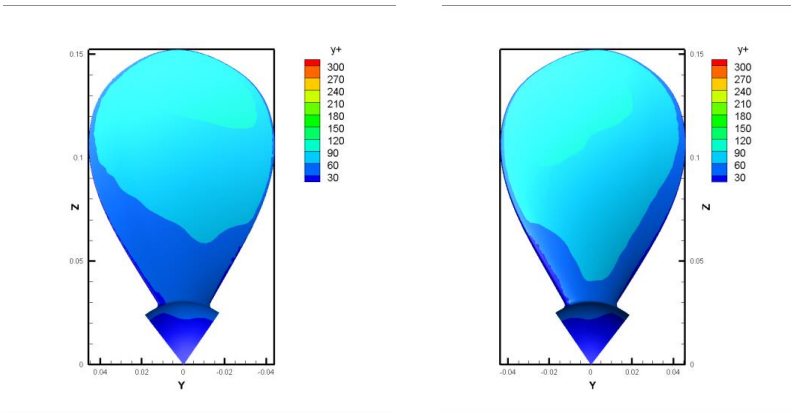


Figure 9.  $y^+$  distribution around DTMB 4381 for  $J=1.0$ .

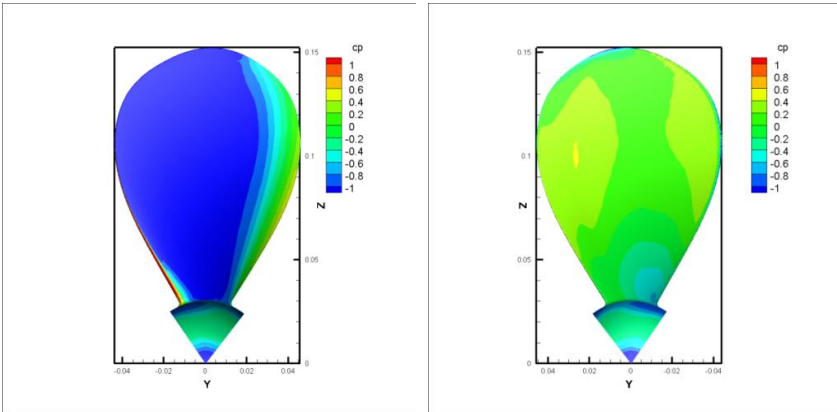


Figure 10.  $c_p$  distribution around DTMB 4381 for  $J=0.889$ .

## 5. Conclusion

In this study, the open water performance factors of DTMB 4381 propeller (the standard test propeller) have been investigated by using a nonlinear blade element momentum and RANS methods. The results have been compared with open water propeller experimental test results. It has been found that the nonlinear blade element momentum theory and the RANS method have given very satisfactory results. Note that nonlinear BEM method is very fast and practical than RANS method.

For low advanced ratios, it has been observed that the relative difference between the results of experimental data and nonlinear BEM method has increased. This difference at low advanced ratio may be caused by the inability to model the stall phenomena under potential flow theory. Given that the potential flow theory does not model the stall situation, the  $C_L$  and  $C_D$  values of the sections required for the BEM method can be obtained by CFD method instead of the XFOIL program, resulting in more precise results.

## 6. References

- Bal, S. (2011a). A method for optimum cavitating ship propellers. *Turkish Journal of Engineering and Environmental Sciences (TUBITAK)*, 35, 139-158.
- Bal, S. (2011b). Practical technique for improvement of open water propeller performance. *Proceedings of the Institution of Mechanical Engineers, Part M, Journal of Engineering for the Maritime Environment*, 225(4), 375-386.
- Bal, S. and Guner, M. (2009). Performance analysis of podded propulsors. *Ocean Engineering*, 36, 556-563.
- Benini, E. (2004). Significance of blade element theory in performance prediction of marine propellers. *Ocean Engineering*, 31, 957–974.
- Brizzolara, S., Villa, D., Stefano, G. (2008) A systematic comparison between RANS and Panel Methods for Propeller Analysis, *Proceedings of 8th International Conference on Hydrodynamics, Nantes, France.*
- Carlton J. S. (2012). *Marine propellers and propulsion*, Butterworth-Heinemann, Burlington, USA, 3rd edition.
- Celik, I. B., Ghia, U., and Roache, P. J. (2008). "Procedure for estimation and reporting of uncertainty due to discretization in CFD applications," *J. Fluids Eng.-Trans. ASME*.
- Fluent 17.2 User's Manual (2016).
- Grassi, D. and Brizzolara, S. (2007). Numerical analysis of propeller performance by lifting surface theory. *2<sup>nd</sup> Int. Conf. on Marine Research and Transportation*, June, Italy.
- Glauert, H. (1935). *Airplane propellers. Aerodynamic Theory.*, Springer, Berlin, Heidelberg, 169–360.
- ITTC (2011). "75-03-01-04 CFD, General CFD Verification," *ITTC-Recomm. Proced. Guidelines*.
- Karaalioglu, M., S. and Bal, S. (2018). Nonlinear correction to blade element momentum theory for marine propellers. *Proc. 3rd International Symposium on Naval Architecture and Maritime (INT-NAM 2018)*, pp: 917-926, Yildiz Technical University, Besiktas Campus, Istanbul, April 24-25.
- McCormick, B. W. (1999). *Aerodynamics of V/STOL flight*, Dover Publications, Mineola, NY.

Molland, A., Turnock, S., and Hudson, D. (2011). Ship resistance and propulsion: practical estimation of ship propulsive power. Cambridge Univ. Press., UK.

Okulov, V., Sørensen, J., and Wood, D. (2015). The rotor theories by professor Joukowsky: vortex theories. *Progress in Aerospace Sciences*, 73, 19–46.

Roache, P. J. (1998). "Verification of Codes and Calculations," *AIAA J.*, 36, 696–702. doi:10.2514/2.457

Soydan, A. (2018). Investigation of marine propeller performance characteristic with blade element momentum theory and computational fluid dynamics. MSc Thesis, Istanbul Technical University.

Soydan, A. and Bal, S. (2018). Nonlinear large angle solution of blade element momentum theory for marine propellers. *Proc. 4<sup>th</sup> Int. Conf. on Advances in Mechanical Engineering, ICAME 2018*, 960-974, Dec. 19-21, Istanbul, Turkey.

Sun, Z., Chen, J., Shen, W. and Zhu, W. (2016). Improved blade element momentum theory for wind turbine aerodynamic computations. *Renewable Energy*, 96, 824–831.

Ulgen, K., (2017). Comparison between blade element momentum theory and computational fluid dynamics methods for performance prediction of marine propellers. MSc Thesis, Istanbul Technical University.

Url-1 <http://web.mit.edu/drela/Public/web/xfoil/>, accessed at: 25.08.2018.

Versteeg, H.K., Malalasekera, W., (2007). *An Introduction to Computational Fluid Dynamics*, 2nd Edition, Pearson.

Whitmore, S.A. and Merrill, R.S. (2012). Nonlinear large angle solutions of the blade element momentum theory propeller equations. *Journal of Aircraft*, 49(4).

Wilcox, D.C., (1993). *Turbulence modelling for CFD*, La Canada.